# The Impact of Simplifications when Modelling Solar Radiation at Large Zenith Angles

Jack Carlin
Blackett Laboratory
Imperial College London, SW7 2AZ
February 11, 2020

***Abstract*—This reports documents the current basic convention for modelling solar radiation changes across a range of solar zenith angles, and subsequently outlining the impact of the simplifications that are imposed onto the original model. As a result, a new model was developed in order to account for the assumptions made in the previous and checked against collected data of the intensity of solar flux over the course of a day. It was revealed that the original model showed a very weak chi-squared confidence in modelling the data, on the order of magnitude of $10^{-113}$. Whereas, our model was able to show a strong improvement to that confidence, reaching 0.2%. The report will outline the composition of the improvements, and where our own methodology lead to their own limitations.**

## I. Introduction

THE aim of this experiment was originally intended to be focused on the variation of measured solar radiation with different cloud types passing over the direct view of the Sun, and possibly use the information to draw conclusions on the nature of clouds or the atmosphere's effect on the Earth's energy budget. However, when using the conventional model it was clear that there were inaccuracies, which could be corrected with re-derivation without the plethora of simplifications applied to the original model.

In general solar radiation models are important within meteorology and helping to improve the output of solar energy infrastructure, given that photovoltaics are the largest growing energy sector globally [1]. Thus, studying the variation in incident solar flux over a range of solar positions can help to predict and meet demands in energy usage.

Throughout the course of this report, the conventional theory will be introduced and it will be shown how it motivated the research techniques and subsequently where it became limiting to the results obtained. Consequently, a new *three-part* novel method will be introduced; showing how it made up for prior pitfalls by reconsidering the original assumptions, upon which the conventional method is built.

## II. Theoretical Background

The cornerstone of the conventional model is the Beer-Bouger-Lambert Law, which looks to describe the intensity, $I_\lambda$ at a specific wavelength, $\lambda$, travelling through a completely absorbing medium of thickness $dl$. The resultant intensity is $I_\lambda + dI_\lambda$, given by:

$$dI_\lambda = -\sigma_{\lambda a} I_\lambda n dl, \tag{1}$$

where $\sigma_{\lambda a}$ is the absorption cross section of a particle at $\lambda$, whilst $n$ is the number density of said particles. In order to simplify the expression, an element of the path that the light takes in the atmosphere, $dl$, can be approximately placed in terms of the Solar Zenith Angle, $Z$. Furthermore, a simple addition to the cross-section parameter can account for scattering effects as well as absorption by assuming they occur simultaneously and that once scattered they are subsequently absorbed; $\sigma_\lambda = \sigma_{\lambda a} + \sigma_{\lambda s}$, where $\sigma_{\lambda s}$ is the scattering cross-section. By saying that $dl = \sec(Z)dz$, where $dz$ is an element of perpendicular altitude, in combination with the derivative in Eq. 1 and a new cross-section, a description of the intensity profile with varying zenith angle comes out as

$$I_\lambda = I_{\lambda 0} \exp\Big[ -\int_l \sigma_\lambda n dl \Big] = I_{\lambda 0} e^{-u \sec(Z)}, \tag{2}$$

where $u$ is the optical depth of the column which encompasses the path, $l$, and is defined as $\int_0^\infty \sigma_\lambda n dz$. This characteristic equation describes the clear sky model for incident solar radiation intensity, however, it makes three key assumptions in order to get there:

1) The atmosphere is a flat medium as opposed to spherical.
2) The atmosphere is isothermal, meaning pressure is strictly exponential.
3) The light path is not refracted throughout the medium.

The atmosphere is not made up of one type of particle and instead is a composition of a vast array of molecules, all with different sizes. On average, these will be fairly small compared to the wavelength of the incident light and thus result in a minor scattering, which is governed by a Rayleigh Scattering model, described by

$$\sigma_{\lambda s} = \alpha^2 \frac{128\pi^5}{3\lambda^4}, \tag{3}$$

where another molecule-specific parameter is the polarisability of the scatterer, $\alpha$. For larger scatterers such as cloud droplets or aerosols (more abundant in cities), the Mie Scattering will govern the interactions where a new variable is introduced in the liquid water path, however that implementation was beyond the scope of this particular investigation.

The Beer-Bouger-Lambert Law only holds for clear sky conditions as there is no longer a clear path for the light to take and thus multiple scattering events will take place as light passes through the atmosphere. This process can be parameterised to model the effect that cloud cover has on the

incident solar flux. One such study, carried out in 2004, was able to empirically derive a mathematical description of the transmittance, trc of a cloud predominantly in terms of the clouds optical density, $u$, and the solar zenith angle, $Z$. The parameterisation took the form of

$$\text{trc} = \frac{a(u) + b(u)\cos(Z)}{1 + (c - d\alpha)u}, \tag{4}$$

where $a(u)$ and $b(u)$ are coefficients that vary with $u$, $\alpha$ is the surface albedo, and $c$ and $d$ remain as empirical coefficients [2]. The functional coefficients, $a$ and $b$, are also mostly constant, however they do vary in the limit u $\rightarrow$ 0, which can be ignored for this investigation despite their behaviour being documented in the same study.

## III. Methodology

The data for the investigation was obtained between January the 13th to the 27th, whilst also split between two sites, Imperial College London's Blackett Laboratory and Hyde Park in South West London. In order to collect the data, two key pieces of apparatus were used, a tripod-mounted solarimeter and a handheld lightmeter. Despite serving a very similar purpose, these two instruments were mechanically quite different; the solarimeter was a thermopile and as such received a broader range of signals from the incident radiation, from 0.3 to 2 $\mu$m, reaching into the IR domain. Whereas, the lightmeter was a photodiode-based optical sensor and so was far stricter with its reception range, spanning from 0.4 to 0.7 $\mu$m. Additionally, they did not output the same units for their readings, the solarimeter displayed the signal in term of mV, but the lightmeter displayed it in kLux. For the solarimeter, the conversion between volts and irradiance in W/m$^2$ was a trivial proportionality of 14.98 $\mu$V(W/m$^2$)$^{-1}$, quoted by manufacturer [3]. On the other hand, the conversion between kLux and W/m$^2$ proved problematic as it is dependent on the wavelength range, however due to the blackbody distribution of the Sun being well documented, the conversion factor could be approximated to 7.9 kLux(W/m$^2$)$^{-1}$ [4].

Another key part of the methodology was to account for diffusive flux. The models described in the previous section pertain to the direct flux from the Sun, incident on a position on Earth, however the instruments will pick up photons reflected from parts of the atmosphere or obstacles such as trees. As a result, the instruments were placed at the data collecting sites with ample open space as to not obstruct the direct solar flux and to reduce the effect of reflected light paths as much as possible. Consequently, it was deemed necessary to couple measurements of all incident flux as well as slightly covering the detectors with a thick object and continuing to take measurements in order to find an approximate order of magnitude for the offset.

## IV. Results

Data was collected over days with clear conditions or strongly overcast and there was very little middle ground between the two within the research time. The data was in the form of radiation readings generally every 5 minutes, and so when it was processed the time on a specific day at a specific location would have to be converted to a solar zenith angle. This was achieved through the use of `PySolar`, a Python package which has a function to find solar zenith angles with the required arguments using a method outlined in a Harvard-led study in 1988 [5]. It was then possible to sweep through the data to find relationships between the direct flux and the zenith angle, a relationship that can be seen in Fig. 1. The

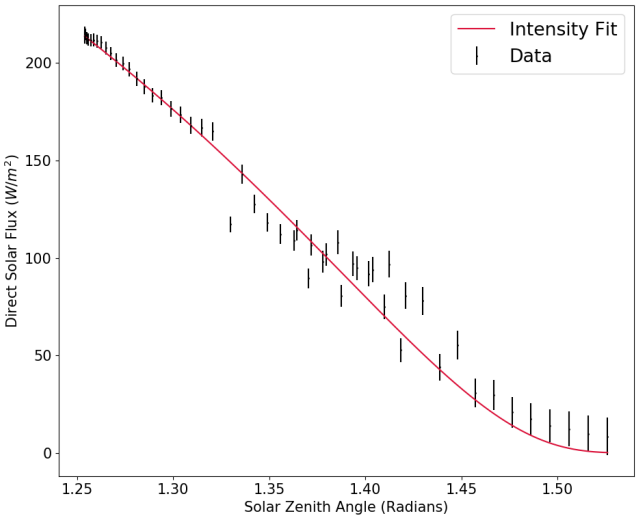


Fig. 1. The data is shown with the simplified Beer-Bouger-Lambert Law overlaid using a least-squares minimisation. The error bars were evaluated by considering the dominance of the diffusive flux and accounting for extrapolation where data points have not been coupled. Attention should be drawn to the weak fit for the high zenith angles.

clear data was collected over three different days and then sorted into the zenith angles; the intensity model described in Eq. 2 was fit onto the data using a Levenberg-Marquadt algorithm to exact a least-squares minimisation. From the minimisation, the parameters for the maximum intensity, $I_{\lambda 0}$, and the cloud optical depth, $u$, were approximated as 694$\pm$15 W/m$^2$ and 0.367$\pm$0.006, respectively. The value obtained for the atmospheric optical density is what was expected, in that it is smaller than 1. Furthermore the value seems to correspond with a study carried out in 1955 at the University of California where the optical depth of the atmosphere above San Diego was measured to be 0.1181 [6]; the order of magnitudes corroborate whilst the factor of three difference would come from the increase in the optical density of the aerosol volume in the atmosphere due to anthropogenic effects over the latter half of the 20th Century [7].

As aforementioned, the model applies for direct flux from the Sun, so the data shown in Fig. 1 has the values measured for diffusive flux removed. On average the proportion was reasonably constant throughout the whole range of zenith angles, where the value of the total reading that was approximately sourced from the diffusion was $\sim$22.2%. However, not all the days measured on were clear, and as cloud cover increases naturally that proportion tends to 100%. Data collected in overcast conditions can be seen represented similarly in Fig. 2; the graph shows a notable dampening in intensity and far more accentuated variability in the raw data. In this case, the peak

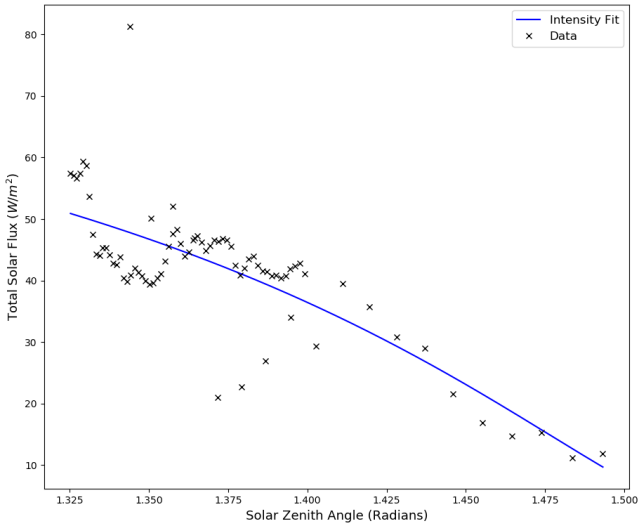


Fig. 2. Once again the raw data is displayed and overlaid with a least-squares fit of the theoretical intensity profile. It is worth noting that the irregular sampling of the data seems to result in a cluster in the lower zenith angles, however this is due to an auxiliary investigation where the data was sampled every minute, which only led to showing the extent of the variability due to cloud cover.

intensity could be found in the same way as before, resulting in $I_{\lambda 0}$ = 111±13 W/m$^2$. For the optical depth however, the same method does not apply because it is constantly changing in overcast conditions.

This is where Eq. 4 became applicable in modelling the changes in optical depth; by assuming the optical depths will be much more than unity and that the transmissivity, trc, was approximately the ratio of the intensity for cloud cover with intensity in clear sky at the same zenith angle, Eq, 4 could be rearranged to find a profile for the optical depth as a function of solar zenith angle.

The large variation in intensity due to fast changes in cloud type cover means that any model for residual solar flux cannot predict future solar radiation changes solely with the presented models without highly inaccurate extrapolation. This meant that the cloud cover data was not used moving forward when investigating the limitation of the models at large zenith angles. Despite a similar divergence from the model found at large angles shown in Fig. 2, we decided to focus completely on the goodness of the clear sky data to the intensity fit because an improved model in the clear sky case can actually be used for prediction, whereas the inaccuracies in the model are less pronounced due to the inherent randomness of the cloud type.

## V. Improvements to the Model

As aforementioned in Section II, the conventional model makes three key assumptions, all of which seem to slightly break down at higher zenith angles. With the atmosphere being curved instead of flat, when the light rays come in at a larger zenith angle, the path they take are modelled differently, and in addition to the isothermal assumption, the pressure variation with altitude will also change due to a different form of a atmospheric volume parcel. Lastly, the conventional model does not account for the refraction of the light path as it enters the atmosphere which has become a staple adjustment in modern technology in order to improve services such as GPS.

### A. Geometric Correction

The fundamental change to the conventional model is the geometric correction which involves taking into account the spherical form for the geometry of the light path, and thus how that may change the intensity profile. Beforehand the intensity profile was derived using an integral with respect to the path, $l$, which was then approximated in the form of the flat altitude, $z$. However, considering the curvature allowed us to derive the change in $l$, with respect to the radial height above the Earth's centre:

$$\frac{dl}{dr} = \frac{(r + R_\oplus)(1 + \cot Z)^{\frac{1}{2}}}{x(1 + \cot^2 Z) + R_\oplus \cot Z}, \tag{5}$$

where $r$ is the radial height and $R_\oplus$ is the radius of the Earth. This derivative allows us to change the exponential integral, from integrating over a domain of the flat altitude to a domain of radial height,

$$\int_l \sigma_\lambda n dl = \int_0^r \sigma_\lambda n \frac{dl}{dr} dr. \tag{6}$$

In turn this will change the intensity profile, a change that can be seen in Fig. 3. In order to solve the differential equation, a RK4 method was employed which is stable under decaying relationships as well as having a reasonable small inherent uncertainty.

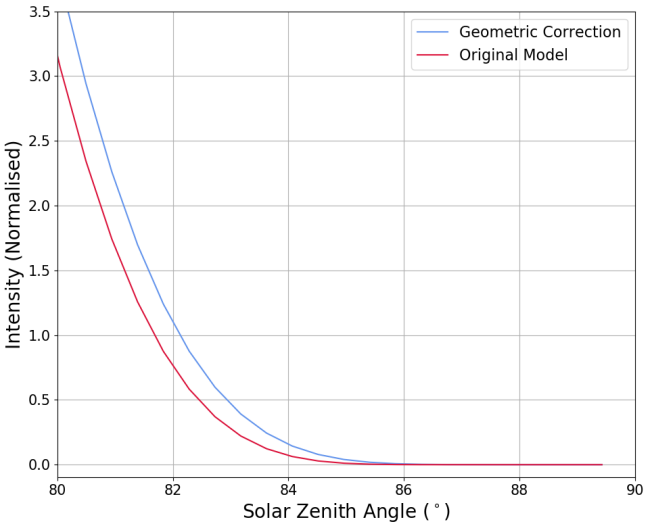


Fig. 3. The intensity profile varying with solar zenith angle of both the original model and the geometric correction. The range is only in the 'high' zenith angles defined as over 80°. The geometric correction still tends to zero despite doing so at a slower rate.

Fig. 4 shows that at high zenith angles, the conventional model underestimates the intensity. This is a general theme throughout the different corrections as originally the exponent in Eq. 2 uses a negative $\sec(Z)$, which goes to infinity, resulting in a zero intensity at 90° and as such in unrealistic. However, despite correcting the original model to a larger value, the slope of intensity with respect to zenith angle seems to be very similar.

### B. Spherical Correction

The spherical correction is an encompassing large scale correction which includes the geometric correction as well as a correction of the pressure. As indicated previously, the conventional model assumes that the atmosphere is isothermal (a simple exponential pressure-altitude relationship), which is a significant assumption as the troposphere has the fastest temperature decline due to its dependence on convective effects. In order to model a corrected atmospheric pressure variation we must consider the pressure difference, $dP$, between the top and bottom of a small volume element of the atmosphere with a radius, $dr$. By resolving the pressure change we can obtain a differential equation to describe the system,

$$\frac{dP}{dr} = -P\Big(\frac{2}{r} + \frac{GMm}{r^2 k_B T(r)}\Big), \tag{7}$$

where $G$ is the gravitational constant, $M$ is the mass of the Earth, $m$ is the average mass of a particle in the atmosphere, $k_B$ is the Boltzmann constant, and $T(r)$ is the new empirical relationship of temperature with altitude, sourced from a study in 1975 [8]. Solving this using a similar RK4 method as in Section V.A, we can find the difference in pressure variation between the conventional and our new adjusted method, although it is also possible to further describe the atmospheric composition by using the ideal gas law to transform the pressure profile to a number density profile. Both metrics, pressure and number density, were compared to their previous forms in the original model and Fig. 4 introduces the 'error' of the original model. The error in this case describes the deviation of our new model compared to the original.

Pressure is shown to be underestimated within the troposphere, likely due to the sharp drop in temperature with altitude [9]. However from that point the pressure is larger in the conventional model, increasing to a peak at a height of 120 km; roughly the boundary between the mesosphere and the troposphere, which is 30 km beyond the Kármán line [10]. On the other hand, the number density seems to be constantly smaller than its true form in the original model, with a sharp trough at 10 km. Only within a 40 km shell at the beginning of the thermosphere is the number density overestimated, yet this is such a small deviation it may be down to the limitations of our own model and not indicate the deviation from the true value.

Combining our pressure correction with the geometric correction shown above, we are able to model the system with a total *spherical correction*. The difference in the intensity profiles between the spherical correction and the original approximation can be seen in similar fashion in Fig. 5, where at first it may seem out of trend with the previous comparison, which showed that the original model underestimates the intensity at high zenith angles.

Nonetheless, this is still the case shown in Fig. 5. The intensity has a lower starting value because the number density of the atmosphere in the spherically corrected model is now much higher meaning the atmosphere is thicker and transmits less flux. If the starting intensity was standardised, the original model would show a faster decay because it has a larger negative slope at high zenith angle dependencies.

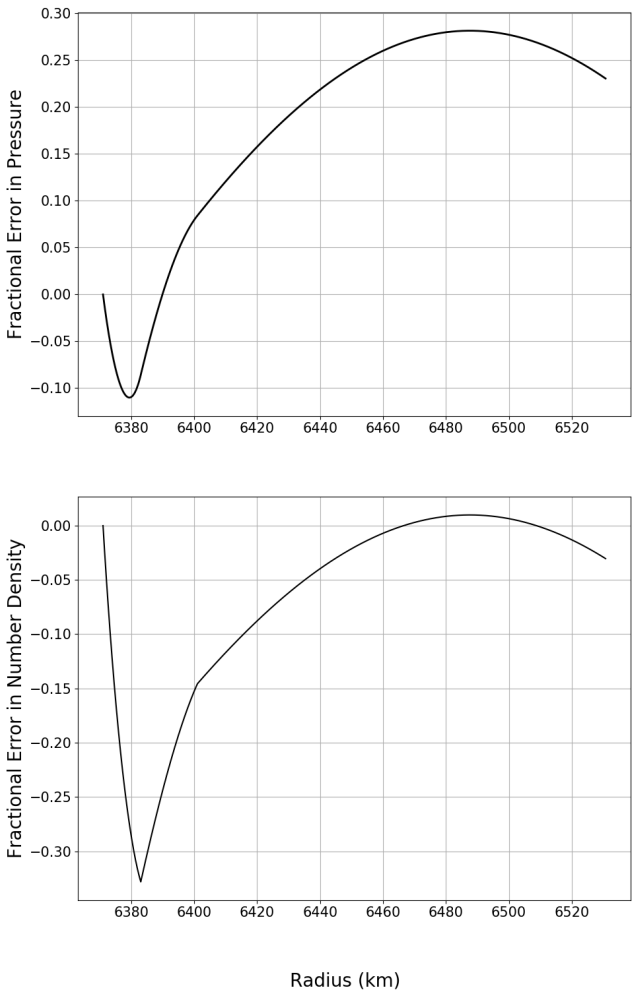


Fig. 4. The fractional difference between the original model and the new distributions of pressure (above) and atmospheric number density (below), presented as an 'error'. This variation is observed over a range of radial distances from the Earth's center, starting at the surface, which is 6371 km. Originally, the pressure and number density scales exponentially with a some dependence on a scale height, of approximately 7 km. For our model however, you could estimate the dependence with the same form but a larger scale height.

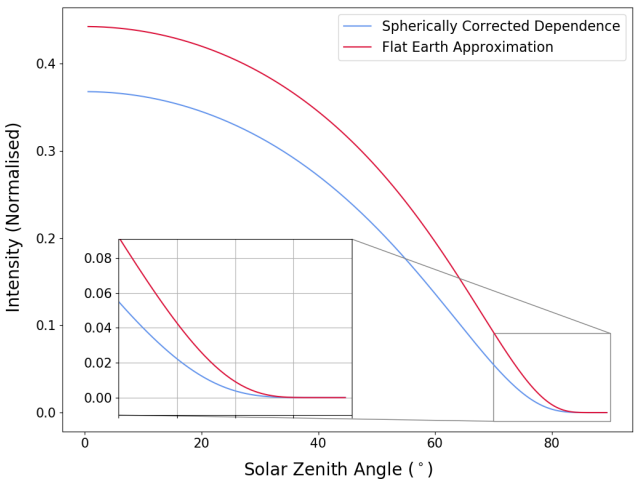


Fig. 5. The normalised intensity for both the new spherical correction and the original (flat-earth) approximation. The inset graph attempts to show difference in slope at high zenith angle dependencies.

### C. Refractivity Correction

The final and possibly most influential correction to the convention is the consideration of the atmospheric refractive index and how that varies over altitude, causing the light path to slightly curve as it comes in.

Atmospheric refractive index is not a constant and instead varies with altitude. The profile of refractivity comes in the form of

$$N = \frac{77.6}{T(r)}\left(P + \frac{4810e}{T(r)}\right), \tag{8}$$

where $N$ is the refractivity, $e$ is the partial pressure of water in air, $T(r)$ is the temperature profile from above. $N$ is defined in terms of the refractive index, $\eta$:

$$\eta = 1 + N \times 10^{-6}. \tag{9}$$

By considering Fermat's Principle, we could then set out to model the light's path through the atmosphere using calculus of variations to minimise the optical path length. This allowed us to derive an integral for the position fo the light path in polar coordinates,

$$\theta_k(r) = \int_{R_\oplus}^{r} \sqrt{\frac{k}{\eta(r)^2 r^4 + k r^2}}\, dr, \tag{10}$$

where $k$ constant, which is varied from 0 to $R_\oplus^2$ in order to determine the path taken and allowing for a range of solar zenith angles from 0° to 90°. The integral was subsequently solved using a trapezium rule method, whilst varying $k$ by selecting a particular zenith angle, $Z$, and comparing it to the angle $\theta_k(d_{Sun})$, where $d_{Sun}$ is the distance to the Sun. Once a value of $k$ is found such that $\theta_k(d_{Sun})$ is within the margin of error for the selected $Z$, which is defined by `PySolar`, then that $k$ is used to solve the integral in Eq. 10.

The new angle distribution allowed for us to make the final adjustment to our improved model. The composite improvements can be seen in Fig. 6, and it is clear that going from the pressure correction in the previous subsection, to the refractivity correction is a reasonably large degree of change. As the original model had intensity tending to zero at a solar zenith angle of 90°, Fig. 7 has the profile reaching very low on the logarithmic scale, and thus the plot consequently shows that the geometric correction has the largest impact at the highest zenith angles. Despite this, the refractivity correction results in the intensity splitting off earlier from the other profiles and so may have a larger impact on the model in totality.

In order to finalise the investigation, all the corrections had to be put together and refitted to the data in order to determine the impact of our corrections on the goodness of the fit. The new fit can be seen in Fig. 7 along with the original fit for the purpose of comparison. In order to compare, we employed a chi-squared test for both the original and the improved fit and looked at both p-values. Furthermore, we deemed it necessary to split up the metrics of goodness into the high solar zenith angles and dependencies and below that mark, which was defined at 80°. The biggest deviation of the data from the original model was beyond that 80°, and so looking at the changes to goodness after that point should be indicative to the success of the investigation.

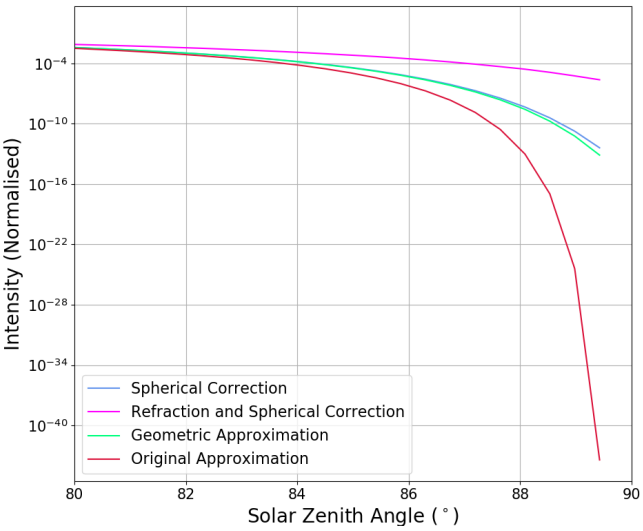


Fig. 6. A plot showing a metric of success for each correction by displaying the variation of intensity at high zenith angles. The metric is loosely based on the value of intensity that the approximations tend to at 90°. All intensities are normalised to have the same value at $Z$=0.

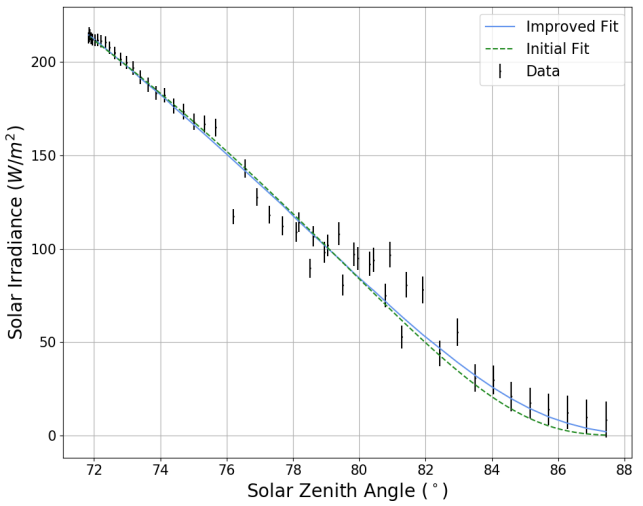


Fig. 7. Apex plot of the investigation showing the comparison of our entire model to the original model when both are minimised to the data introduced in Section IV. The new fit described the very high zenith angle behaviour far better than the original.

Using the aforementioned p-values, we can say that the confidence of the original fit was 98.9% for the range of solar zenith angles prior to 80°, whereas our new model reaches a confidence level of 99.7%. More importantly, the original model shows an extremely poor confidence on the order of $10^{-113}$ at over 80° and so it is fair to say that the original model cannot describe high zenith angle dependence. On the other hand, our model results in a p-value confidence of 0.2%, which may seem very small but in comparison to the conventional model, it is beyond a vast improvement.

Another supporting metric for comparison is the absorption and scattering cross-section, $\sigma_\lambda$, which would change through

the adjustments to the original model. The original model resulted in an effective cross-section of $1.97\pm0.03\times10^{-26}$ cm$^2$. Whilst our own model output a similar cross-section in $2.26\pm0.04\times10^{-26}$ cm$^2$. One possible reason as to why the models show far different confidences but result in a similar cross-section is that the improved model has two offsetting features; a thicker atmosphere described by the spherical correction would result in a larger cross-section, whereas a shorter path through the atmosphere described by the geometric correction would result in a smaller cross-section.

## VI. Conclusion

To conclude, the aim of the experiment was to analyse the limitations that arise by introducing simplifications to a model of solar radiation, which to a large extent, was comfortably achieved. It is clear from this report that the original model with a flat-earth approximation shows strong limitation at high solar zenith angles, displaying a very weak confidence level of $< 10^{-100}$ at that angle range. Fortunately, we were able to use the analysis of the simplifications and develop an improved novel fit, which allowed us to constrain the confidence to 0.2%.

Despite the extreme improvement, the confidence is still low, which is expected due to the large number of factors which would affect solar radiation models. Two evaluations to note: firstly the proportion of diffusive was assumed to be constant, however this would have been an underestimation at very high solar zenith angles. Secondly, and more significantly, the temperature dependence was highly localised and thus did not account for the lateral distribution of temperature.

## Appendix A
## Deriving the Geometric Correction

Define a radial height above the Earth, $r$, as

$$r = \sqrt{x^2 + z^2} - R_\oplus,$$

where $z$ is the normal from a position on Earth and $x$ is the perpendicular. As such the vector of the light path can be defined as

$$\vec{l} = R_\oplus \vec{\hat{z}} + \lambda(\cos(Z)\vec{\hat{z}} + \sin(Z)\vec{\hat{x}}),$$

where $\lambda$ is a positional parameter defining the distance form the surface. By only considering the length of a step along the path, the square of that distance is given by,

$$l^2 = (\lambda\sin(Z))^2 + (\lambda\cos(Z))^2.$$

However, since we know that $x = \lambda\sin(Z)$, we can also say $\lambda\cos(Z) = x\cot(Z)$, which allows us to further simplify and describe the total derivative,

$$dl = dx\sqrt{1 + \cot^2(Z)}.$$

Recalling the original form of $r$, the total derivative, $dr$, can also be found,

$$dr = \frac{x}{\sqrt{x^2+z^2}}dx + \frac{z}{\sqrt{x^2+z^2}}dz.$$

By also recalling that $z = x\cot(Z) + R_\oplus$, and thus $dz = \cot(Z)dx$, the $dz$ dependence can be removed:

$$dr = \frac{x(1+\cot^2(Z)) + R_\oplus\cot(Z)}{r + R_\oplus}dx.$$

Finally the ratio of $dl$ and $dr$ can be computed as

$$\frac{dl}{dr} = \frac{(r+R_\oplus)(1+\cot Z)^{\frac{1}{2}}}{x(r)(1+\cot^2 Z) + R_\oplus\cot Z},$$

where $x(r)$ has the form:

$$x = \sqrt{\frac{r^2}{1+\cot^2(Z)} - \frac{R_\oplus^2}{(1+\cot^2(Z))^2}} - \frac{R_\oplus\cot(Z)}{1+\cot^2(Z)}.$$

## Appendix B
## Deriving the Pressure Correction

Resolving the forces on a spherical volume element in the atmosphere gives a relationship:

$$P_{down}(4\pi r^2) = P_{up}(4\pi(r+dr)^2) + 4\pi r^2\rho g dr,$$

where $P_{down}$ and $P_{up}$ are the pressures associated with a downward and upward force respectively, $\rho$ is the density of a volume element, and $g$ is the gravitational acceleration. Rearranging and saying that $dr^2 \to 0$ allows us to form a differential equation,

$$\frac{dP}{dr} = -P\cdot\frac{2}{r} - \rho g.$$

The density, $\rho$, is governed by the Ideal Gas Law, and thus is a function of pressure $\rho = nm = \frac{P}{k_b T}m$. Thus finalising the differential equation:

$$\frac{dP}{dr} = -P\Big(\frac{2}{r} + \frac{GMm}{r^2 k_B T(r)}\Big).$$

## Appendix C
## Deriving the Refractivity Correction

Considering Fermat's Principle for the optical path, $L$, given by,

$$L = \int_{l_1}^{l_2}\eta dl,$$

where $\eta$ is the refractive index and $dl$ is a small path element. By transforming the integral into terms of $r$, $dl \to \frac{dl}{dr}dr$, we can obtain an expression,

$$L = \int_{R_\oplus}^{d_{Sun}}\eta(r)\sqrt{1+\left(\frac{d\theta}{dr}\right)^2}dr.$$

This can then be solved by considering the calculus of variation because $\theta$ is defined at both limits; by solving the Euler-Lagrange equation for the integrand, the optical path, $L$, can be minimised. This gives,

$$\frac{d}{dr}\left(\frac{\eta(r)r^2\frac{d\theta}{dr}}{\sqrt{1+r^2\left(\frac{d\theta}{dr}\right)^2}}\right) = 0.$$

By integrating and introducing a constant of integration, we can obtain the form for $\theta_k(r)$,

$$\theta_k(r) = \int_{R_\oplus}^{r}\sqrt{\frac{k}{\eta(r)^2r^4 + kr^2}}dr.$$

## REFERENCES


[1] H. E. Murdock, D. Gibb, T. André, F. Appavou, A. Brown, B. Epp, B. Kondev, A. McCrone, E. Musolino, L. Ranalder, *et al.*, "Renewables 2019 global status report," 2019.

[2] M. F. Fitzpatrick, R. E. Brandt, and S. G. Warren, "Transmission of solar radiation by clouds over snow and ice surfaces: A parameterization in terms of optical depth, solar zenith angle, and surface albedo," *Journal of climate*, vol. 17, no. 2, pp. 266–275, 2004.

[3] K. und Zonen, *CMP Series Instruction Manual*, 2016. [Online]. Available: https : / / www . kippzonen . com / Product/12/CMP6-Pyranometer.

[4] P. Michael, *A conversion guide: Solar irradiance and lux illuminance*, 2019. DOI: 10 . 21227 / mxr7 - p365. [Online]. Available: http://dx.doi.org/10.21227/mxr7-p365.

[5] P. Bretagnon and G. Francou, "Planetary theories in rectangular and spherical variables-vsop 87 solutions," *Astronomy and astrophysics*, vol. 202, pp. 309–315, 1988.

[6] D. Deirmendjian and Z. Sekera, "Global radiation resulting from multiple scattering in a rayleigh atmosphere," *Tellus*, vol. 6, no. 4, pp. 382–398, 1954.

[7] Y. Xue, X. He, G. de Leeuw, L. Mei, Y. Che, W. Rippin, J. Guang, and Y. Hu, "Long-time series aerosol optical depth retrieval from avhrr data over land in north china and central europe," *Remote Sensing of Environment*, vol. 198, pp. 471–489, 2017.

[8] J. Waters, K. Kunzi, R. Pettyjohn, R. Poon, and D. Staelin, "Remote sensing of atmospheric temperature profiles with the nimbus 5 microwave spectrometer," *Journal of the Atmospheric Sciences*, vol. 32, no. 10, pp. 1953–1969, 1975.

[9] K. S. Arnold and C. She, "Metal fluorescence lidar (light detection and ranging) and the middle atmosphere," *Contemporary Physics*, vol. 44, no. 1, pp. 35–49, 2003.

[10] J. C. McDowell, "The edge of space: Revisiting the karman line," *Acta Astronautica*, vol. 151, pp. 668–677, 2018.